



This is a repository copy of *Supraglacial weathering crust dynamics inferred from cryoconite hole hydrology*.

White Rose Research Online URL for this paper:
<http://eprints.whiterose.ac.uk/95245/>

Version: Accepted Version

Article:

Cook, J.M., Hodson, A.J. and Irvine-Fynn, T.D.L. (2016) Supraglacial weathering crust dynamics inferred from cryoconite hole hydrology. *Hydrological Processes*, 30 (3). pp. 433-446. ISSN 0885-6087

<https://doi.org/10.1002/hyp.10602>

This is the peer reviewed version of the following article: Cook, J. M., Hodson, A. J., and Irvine-Fynn, T. D. L. (2016) Supraglacial weathering crust dynamics inferred from cryoconite hole hydrology. *Hydrological Processes*, 30: 433–446, which has been published in final form at <http://dx.doi.org/10.1002/hyp.10602>. This article may be used for non-commercial purposes in accordance with Wiley Terms and Conditions for Self-Archiving (<http://olabout.wiley.com/WileyCDA/Section/id-820227.html>).

Reuse

Unless indicated otherwise, fulltext items are protected by copyright with all rights reserved. The copyright exception in section 29 of the Copyright, Designs and Patents Act 1988 allows the making of a single copy solely for the purpose of non-commercial research or private study within the limits of fair dealing. The publisher or other rights-holder may allow further reproduction and re-use of this version - refer to the White Rose Research Online record for this item. Where records identify the publisher as the copyright holder, users can verify any specific terms of use on the publisher's website.

Takedown

If you consider content in White Rose Research Online to be in breach of UK law, please notify us by emailing eprints@whiterose.ac.uk including the URL of the record and the reason for the withdrawal request.



eprints@whiterose.ac.uk
<https://eprints.whiterose.ac.uk/>

1 **Supraglacial weathering crust dynamics inferred from cryoconite hole hydrology**

2 **J.M.Cook¹, A. J. Hodson^{2,3}, T.D.L. Irvine-Fynn⁴**

3 1 – College of Life and Natural Sciences, University of Derby, Derby, DE22 1GB

4 2 – Department of Geography, University of Sheffield, Sheffield, S10 2TN

5 3 – Arctic Geology, University Centre in Svalbard, Longyearbyen, Norway

6 4 – Centre for Glaciology, Aberystwyth University, Aberystwyth SY23 3DB.

7
8 **Corresponding Author: J M Cook, j.cook1@derby.ac.uk**

9
10
11
12
13
14
15
16
17
18
19
20
21
22
23
24
25
26
27
28
29
30
31
32
33

34 Introduction

35 Building upon work by Muller and Keeler (1969), Irvine-Fynn and Edwards (2014) examined the
36 ecological role and significance of the “weathering crust” - the shallow (~2 m) layer of porous ice that
37 develops seasonally over ablating glacier surfaces. They asserted that, excluding Antarctica, global
38 glacial weathering crusts may support some 10^{21} to 10^{26} microbes (Irvine-Fynn & Edwards, 2014),
39 representing an important yet poorly understood component of supraglacial ecosystems. Hydrological
40 fluxes through the weathering crust may profoundly influence in situ microbial communities
41 (Edwards et al. 2011), export of microbial cells from glacier surfaces (Irvine-Fynn et al., 2012) and
42 biodiversity in glacier-fed streams (Wilhelm et al., 2013), making the hydrological behaviour of the
43 weathering crust an important area of research. Despite previous researchers directing attention to
44 supraglacial hydrology (e.g. Derikx, 1971; Munro, 2011), surprisingly little literature exists directly
45 examining water movement through near-surface ice (e.g. Theakstone & Knudsen, 1981; Karlstrom et
46 al. 2014).

47 The weathering crust forms due to subsurface melt from shortwave radiation (I^*), the attenuation of
48 which typically limits subsurface melting on glaciers to within a “photic zone” (Irvine-Fynn &
49 Edwards, 2014) a few tens of centimetres thick (Shumskii, 1964), but can extend to greater depths
50 defined by Beer’s Law, which describes the exponential decay of solar radiation as a function of
51 distance through ice (Oke, 1987):

$$52 \quad I_z^* = I_0^* e^{-kz} \quad (\text{Eq.1})$$

53 where I_z^* is the shortwave incident radiation at depth z , I_0^* is the radiation flux at the ice surface and k
54 is the extinction coefficient. Values of k vary in supraglacial ecosystems (Hodson et al. 2013), but
55 typically lie in the range $2.00 - 20.00 \text{ m}^{-1}$ for optically clear (blue) glacier ice and dry snow
56 respectively (Hodson et al. 2013). By contrast, the value for pure ice is $\sim 6.00 \times 10^{-4} \text{ m}^{-1}$ (Geiger,
57 1965). The dissipation of radiative energy in the photic zone leads to subsurface melting, enlarging
58 interstitial spaces and disaggregating ice crystals. Additionally, heat flow within the interstitial space
59 further contributes to the declining cohesion of the near-surface ice crystals (Nye, 1991). This
60 decaying surface has been referred to as “honeycomb ice” (e.g. Zeng et al. 1984; Cutler & Munro,
61 1996), and detailed energy balance studies have demonstrated the relative importance of the
62 subsurface melt volume (see Munro, 1990; Wheler and Flowers, 2011). Near-surface ice exhibits a
63 characteristic non-linear trend of increasing ice density with depth (LaChapelle, 1959; 1961): from a
64 highly porous surface (300 kg m^{-3} : Shumskii, 1964; Schuster, 2001) to a dense subsurface of $\sim 900 \text{ kg}$
65 m^{-3} .

66 Muller & Keeler (1969) indicated a meteorological control on weathering crust evolution: maximum
67 rates of weathering crust formation are associated with clear sky conditions that allow I^* to dominate
68 the surface energy balance. During such periods the overall porosity of the near-surface ice
69 progressively increases, and the weathering crust expands vertically to greater depth. Consequently,
70 through increased porosity, the weathering crust becomes a location for storage of meltwater (Larson,
71 1978; Liestøl et al. 1980; Irvine-Fynn et al. 2006; Irvine-Fynn, 2008), controlling near-surface
72 drainage velocities (Wakahama et al. 1973; Larsen, 1977; Shea et al. 2005; Munro, 2011), and
73 providing a substrate vulnerable to supraglacial rill initiation (Schuster, 2001). Recent work by
74 Karlstrom et al. (2014) connected microscale weathering crust hydraulics to macroscale supraglacial
75 meltwater flow features and indicated a research imperative is to improve current understanding of the
76 dynamics of sub-surface flow.

77 During synoptic periods of cloud cover, high air temperatures and high wind speeds, the surface
78 energy balance can become dominated by turbulent heat fluxes. This has a three-fold effect: first,
79 selective radiation-driven subsurface melting can decrease or stop; second, refreezing of melt water in
80 interstitial pore spaces can occur; and third, low density surface-ice ablates through convective
81 melting. These processes cause the weathering crust to decay rapidly (Muller and Keeler, 1969;
82 Schuster, 2001). Energy input by rainfall may also contribute to the removal of porous weathering
83 crust ice (Muller & Keeler, 1969), although this method of ablation is often assumed negligible

84 (Rothlisberger and Lang, 1987). With decreased porosity, the role of the weathering crust in
85 hydrologic transmission and storage soon diminishes. As a depth limited aquifer, the dynamic
86 weathering crust's dynamic impact on supraglacial hydrographs at short (sub-hourly) to seasonal
87 time-scales is, therefore, complex and remains largely unexplored (Irvine-Fynn et al. 2011).

88 As highlighted by Muller and Keeler (1969) and Irvine-Fynn & Edwards (2014), the weathering crust
89 provides the substrate for the development of cryoconite holes. These are pits with quasi-circular
90 planforms that develop on ice surfaces worldwide due to enhanced ablation under patches of
91 biologically inoculated sediment. They have been recognised as areas of high biodiversity and
92 microbial activity due to the relatively stable, well-illuminated and nutrient-rich environments they
93 offer microbes (e.g. McIntyre, 1984; Wharton, 1985; Hodson et al. 2008; Cook et al. 2010; Edwards
94 et al. 2013a). Despite cryoconite holes traditionally being viewed as discrete microbial habitats (e.g.
95 Wharton et al. 1985), they generally contain a column of melt water which may exhibit stratified
96 populations of protozoa (Mieczan et al. 2013), and are likely hydrologically connected to the
97 weathering crust aquifer. There is currently a paucity of literature concerning hydrological processes
98 operating within cryoconite holes and their role in the wider weathering crust hydraulic regime.

99 To date, most research into cryoconite hole hydrology has been limited to Antarctica (e.g. Tranter et
100 al. 2004; Fountain et al. 2004; Bagshaw et al. 2007; MacDonnell and Fitzsimons, 2008; Hodson et al.
101 2013) where low surface temperatures promote the formation of thick ice lids that decouple
102 cryoconite holes from hydrological, microbiological, gaseous and sedimentological exchanges with
103 the atmosphere and glacier surface. Critically, in Antarctica, where low air temperatures inhibit
104 surface melting, internal subsurface melting by shortwave radiation penetration occurs due to a "solid
105 state greenhouse effect" (Brandt and Warren, 1993; Liston et al. 1999). Weathering crust development
106 processes here contrast to those described above, and work by Hoffman et al. (2014) suggests that this
107 only has an appreciable impact upon glacier runoff when melt water efficiently drains through the
108 weathering crust, else it simply refreezes in situ. Consequently, while Antarctic cryoconite holes may
109 connect to each other via discrete subsurface conduits (MacDonnell and Fitzsimons, 2008), the
110 subsurface drainage mechanism is likely unique to cold Antarctic glaciers (Fountain et al. 2004;
111 Hodson et al. 2013). Contrastingly, in Arctic latitudes, cryoconite holes penetrate weathered ice at
112 melting point and generally maintain an open interface with the atmosphere during the ablation
113 season. This suggests that Arctic cryoconite holes probably differ in their hydrologic regime and play
114 a different role in weathering crust hydrology than their austral equivalents. However, MacDonnell
115 and Fitzsimons (2012) described intergranular drainage development around Antarctic cryoconite
116 holes, suggesting some commonality in the drivers of weathering crust dynamics globally.

117 In Arctic settings, the lack of isolation by ice lids has been linked to different biotic communities
118 compared with those in the Antarctic, due to frequent mixing and flushing with meltwater (Meuller
119 and Pollard, 2004) and greater inputs of allochthonous biota (Paultier et al. 2013). Furthermore, an
120 active supraglacial hydrological system may cause disaggregation (Takeuchi et al. 2000) and
121 redistribution (Hodson et al. 2007; Irvine-Fynn et al. 2011) of cryoconite, influencing microbial
122 activity (Stibal et al. 2012), cyanobacterial filament lengths and therefore cryoconite grain stability
123 (Langford et al. 2014). However, these observations are not independent from the weathering crust,
124 where a reduction in interstitial void spaces in increasingly dense ice establishes a gradient of
125 decreasing hydrologic transmission of labile microbes with depth (Irvine-Fynn & Edwards, 2014).
126 Since the weathering crust is synoptically variable, rates of storage and transmission of water and
127 microbes likely also vary at a range of spatio-temporal scales (Irvine-Fynn et al. 2012). Therefore,
128 coupling weathering crust and cryoconite hole hydrology to inform supraglacial microbiology is a
129 research imperative that remains under-explored. Therefore, the aims of this study were 1) to generate
130 a high resolution time series of hydraulic changes within the weathering crust using cryoconite holes
131 on Austre Brøggerbreen as natural boreholes; 2) to undertake rapid slug and bail tests to determine
132 hydraulic conductivity within the weathering crust; 3) to use these data to make inferences related to
133 the storage and transmission of water and microbes through the weathering crust.

134 **Field site**

135 Field work was conducted at Austre Brøggerbreen (hereafter, AB), Svalbard (78°10'49"N, 15°30'21"E;
136 Fig. 1A) between 9th and 31st August, 2009. Mean annual air temperatures at sea level in the locality are -
137 6.30 °C, with warmest mean monthly temperature of 4.90 °C in July, and mean annual precipitation of 400
138 mm yr⁻¹ (eKlima, 2012). Austre Brøggerbreen is a north-facing valley glacier located on Brøggerhalvøya,
139 with an area of ~9 km². The glacier's catchment extends to ~740 m asl, with ice extending from 60 to 650
140 m asl, and steep slopes extend from the glacier's margin to the catchment watershed in the uppermost
141 elevations. Since 1966, AB has exhibited an almost continuously negative mass balance of -0.60 m w.e.
142 per year (Barrand et al. 2010) with evidence for accelerated thinning in the upper 200 m of the glacier's
143 elevation range since ca. 1990 (James et al. 2012). These recent thinning trends have resulted in AB
144 transitioning from a polythermal to cold-based thermal regime (Nowak & Hodson, 2014).

145 The cold-based glacier is characterised by an extensive supraglacial drainage system, with a number of
146 discrete moulins descending to englacial drainage routes (Vatne, 2001; Stuart et al. 2003; Vatne & Refnes,
147 2003). The recent and consistently negative annual mass balances have progressively exposed
148 unconsolidated sediments at the ice margins, including in the upper ablation and accumulation areas,
149 which may be mobilised on to the glacier surface by snow melt and thaw (Porter et al. 2010). Such sources
150 may supplement aeolian mineral dust deposition and provision cryoconite on AB. Contrasting cryoconite
151 microbial communities have been identified between AB and the adjacent glaciers (Edwards et al. 2011;
152 2013b), and, therefore, the regional representativeness of AB is unclear. Local estimates of cryoconite
153 loading on the adjacent glacier, Midtre Lovénbreen, by Hodson et al. (2007) suggest cryoconite
154 concentrations of up to 10600 kg km⁻² with discrete holes being common in the upper ablation zone.
155 According to research at Waldemarbreen (78°40'0"N, 12°0'0"E), typical depths of the weathering crust
156 for glaciers in this region are limited to ~1 m, with deeper ice remaining below pressure melting point
157 even during summer months (Sobota, 2009). For further details relating to the site's glaciology,
158 hydrometeorology and ecology, see Hagen & Saetrang (1991), Hodson et al. (1998, 2002); Barrand et al.
159 (2010) and Edwards et al., (2011).

160

161 **Methods**

162 The primary data collection at the AB field site focused upon cryoconite hole hydrology, with
163 ancillary data used to describe the hydrometeorology of the ice surface.

164 **Meteorology:**

165 At the study site, boundary layer air temperature (T_a) over the observation period was measured using
166 10 k Ω thermistors sheltered by a Stevenson screen, positioned 1 m above the ice surface. Thermistors
167 were calibrated prior to installation and the Steinhart-Hart equation used to convert resistance to
168 temperature ($r^2 = 0.9998$). In addition a Delta-T ES-2 silicon photodiode was used to measure I^*
169 (across the visible range 400-1050 nm). Data were logged at 5 minute intervals, recording averages of
170 sample measurements made every 30 s.

171 **Time series of cryoconite hole hydrology:**

172 To ascertain variations in water stored within cryoconite holes associated with melt inputs or
173 weathering crust drainage processes, records of water levels in cryoconite holes were acquired. A
174 Delta-T DL2-e data logger was placed centrally and capacitance water level sensors installed in each
175 of eight cryoconite holes (Fig. 1B). All monitored holes were located in ablating ice that was
176 relatively crystallographically homogeneous, in a broadly low gradient area and far from
177 topographical features which might have imposed specific shadowing or large-scale hydrological
178 regimes; however, holes 7 and 8 were proximate to a small meandering supraglacial stream. Average
179 diameter and depth for all holes over the measurement period was 103 mm and 227 mm, respectively,
180 and the average hole water volume (V_w) was 1987 cm³.

181 To monitor variations in V_w , a ‘goalpost’ structure (Fig. 1B) was used to instrument each cryoconite
 182 hole. Two vertical ‘rig poles’ were inserted into pre-drilled holes ca. 20 cm either side of each hole,
 183 and a horizontal ‘crossbar’ used to suspend the capacitance sensors. Submergence of the sensor
 184 resulted in reduced voltage output, which is sensitive to variations in water level with respect to the
 185 probe itself. Calibration revealed a sensor error of + 1 to -2 mm. Sensors which were dry prior to
 186 submergence output a slightly higher voltage (10 - 20 mV higher) than those which had been ‘pre-
 187 wetted’, indicating worst-case errors of 5 mm, independent of temperature, conductivity or ionic
 188 strength of the solution.

189 Water level was logged at 5-minute intervals, averaging measurements made every 30 s. At each hole
 190 at least daily manual measurements of apparent surface ablation and cryoconite hole depth were
 191 gathered and used to monitor the descent of the cryoconite hole system away from the crossbar. This
 192 data was used to correct the water level data for surface ablation. Water level sensors were also
 193 repositioned daily to ensure constant submergence despite surface lowering. The magnitude of the
 194 repositioning was recorded and the data corrected accordingly. Water levels were converted into rate
 195 of volumetric change in the cryoconite hole water between times t_1 and t_2 using Equation 2:

$$196 \quad \Delta V_w = \frac{\pi r_c^2 (h_{wl} - h_{hole} - h_{surf})}{t_2 - t_1} \quad (\text{Eq.2})$$

197 where ΔV_w = change in cryoconite hole water volume, r_c is cryoconite hole radius, and h = changes in
 198 heights of cryoconite hole water meniscus, floor, and glacier ice surface (respectively, subscripts wl,
 199 hole and surf) (Fig 1 B).

200 Hydraulic conductivity in the weathering crust:

201 We used so-called ‘slug-and-bail’ tests to establish the hydraulic conductivity (K) of the weathering
 202 crust: a common technique employed in the study of saturated porous media such as soils (e.g. Bear,
 203 1972; Amoozegar and Warrick, 1986). These were employed at a sample set of cryoconite holes in
 204 the study area. Three slug tests and three bail tests were undertaken in separate cryoconite holes. Each
 205 test was undertaken during the morning at 10am (± 1 hour). Further slug and bail tests were also
 206 undertaken in the afternoon, however the data is omitted here due to recharge being too rapid to
 207 accurately measure. For bail tests a 100 mL syringe was used to extract water in volumes of 400 mL,
 208 1000 mL and 1500 mL, all of which represented a complete drainage of the hole water. For slug tests
 209 water was added using a 100 mL syringe in volumes of 200 mL, 300 mL and 800 mL. Water was
 210 sourced and discarded > 10 m from the test hole to avoid influencing local hydraulic gradients.
 211 Records of ΔV_w were monitored using the capacitance sensors, as described above. Slug and bail data
 212 were used to calculate saturated hydraulic conductivity (K) at five-minute intervals using Equations 2
 213 and 3, adapted from Bouwer and Rice (1976):

$$214 \quad K = \frac{r_c^2 \log\left(\frac{R_e}{r_w}\right)}{2d} \cdot \frac{1}{t} \log\left(\frac{h_0}{h_t}\right) \quad (\text{Eq.2})$$

215 for which:

$$216 \quad \log\left(\frac{R_e}{r_w}\right) = \left[\frac{1.1}{\log\left(\frac{b}{r_w}\right)} + \frac{A+B \log\left[\frac{(D-b)}{r_w}\right]}{\left(\frac{d}{r_w}\right)} \right]^{-1} \quad (\text{Eq.3})$$

217 where r_c = hole radius; R_e = radial distance over which the change in head position is dissipated in the
 218 aquifer; r_w = horizontal distance from centre of well to undisturbed aquifer; d = open well depth
 219 (equal to hole depth); h_0 = water level at t_0 ; h_t = water level at time t_1 ; b = hole depth; D = aquifer
 220 depth. Terms A and B are dimensionless numbers that vary according to the length of the open section
 221 of well and r_w (Bouwer and Rice, 1976). This method was appropriate because it is applicable to both
 222 slug and bail tests for boreholes of any depth and diameter.

223 For cryoconite holes, $d = b$ since no screen was used. Bouwer and Rice (1976) showed that when D
224 $\gg d$, as in cryoconite holes, D has negligible impact on R_e , reporting an effective upper limit for \log
225 $((D - b)/r_w)$ of 6. Therefore, the term $\log ((D - b)/r_w)$ was replaced by the value 6 in Equation 2. It is
226 also assumed that r_w is small, given the small ΔV_w recorded in cryoconite holes, observed rapid
227 dissipation of slug water, and lack of ΔV_w in holes close (< 5 to 20 cm) to those used for slug and bail
228 tests. Although unknown, a value of 5 cm for r_w is conservatively estimated in this study.

229 Melt Modelling:

230 Surface ablation (mm w.e.) at the study area was modelled using Brock and Arnold's (2000) point
231 surface energy balance model. The melt model was driven by meteorological data acquired at the field
232 site between 9th and 31st August 2010. Vapour pressure was calculated from T_a records (see Tetens,
233 1930). Values for local surface ice albedo of 0.4 (after Bruland and Hagen, 2002; Hodson et al. 2008)
234 and roughness of 0.00066 m (after Arnold and Rees, 2003) were used. Optimization of this model is
235 generally accomplished by varying albedo; however, since this is a key parameter in the development
236 of the seasonal weathering crust we ran the model a priori. Due to the absence of wind speed data
237 from AB during the observation period, records from the adjacent, and similarly oriented Midtre
238 Lovénbreen were used.

239 Results

240 Meteorology:

241 Over the observation period, mean T_a and I^* were 0.51 ± 2.14 °C and 198.72 ± 219.90 Wm^{-2}
242 respectively (Fig 2A). These low values reflect the reduced solar angle and declining incident
243 radiation as the Arctic summer approaches termination, coupled with the common occurrence of low
244 clouds (Hanssen-Bauer et al. 1990). Of note, during clear sky conditions (between 17th and 19th
245 August), I^* rose to 1132.20 Wm^{-2} whilst T_a never rose above 8.50 °C. Prior to 20th August and after
246 24th August, night-time T_a dropped below zero; however, from 20th to 24th August T_a remained
247 continually positive. This period is hereafter referred to as the 'Warm Air Phase'. The Warm Air
248 Phase coincided with a period of low I^* , likely resulting from insulation by sustained synoptic cloud
249 cover causing turbulent fluxes to dominate melt processes.

250 Time series of cryoconite hole hydrology:

251 In all eight cryoconite holes, ΔV_w showed clear diurnal fluctuations out of phase with I^* and T_a (Fig. 2B).
252 Measurements from Holes 7 and 8 ended early due to invasion by a migrating supraglacial rill.
253 Importantly, significant linear decreases in V_w over the entire measurement period were recorded in all
254 eight holes, with an average rate of change of -0.0060 $mm^3 s^{-1}$ (equivalent to 0.50 $mL d^{-1}$) and individual
255 coefficients of determination for linear regression models between V_w and time were between 0.73 and
256 0.93 (Table 1) for all except Hole 1. Since the data were corrected daily for both cryoconite hole depth and
257 surface ablation, the linear decrease in V_w over the entire observation period is not a melt or measurement
258 artefact.

259 In Hole 1 diurnal ΔV_w fluctuations were amplified during the Warm Air Phase that followed 20th August;
260 however, this was not observed in any of the other holes. The late season amplification in ΔV_w in Hole 1
261 influenced the overall trend in V_w . In Hole 1 following the warm air phase, V_w changed by up to 44.45
262 cm^3 in 16 hours (between 477 and 493 hours into measurement period; see Fig 2B), almost four times
263 greater than the largest fluctuation in any other hole at any time during the observation period (12.3 cm^3
264 increase in V_w between 414 and 427 hours in Hole 3).

265 Following detrending of the ΔV_w records using linear regression, cross correlation was used to quantify
266 the dominant lag times between V_w and both I^* and T_a in Holes 1-6. The lag times associated with
267 maximum positive Pearson correlation coefficients ("dominant lag") and their associated R values are
268 shown in Table 2A. For ΔV_w and I^* , the mean dominant lag was 15.18 ± 3.13 hr, while the mean
269 dominant lag between ΔV_w at T_a was 16.04 ± 4.27 hr. Data from Holes 7 and 8 were omitted due to their

270 invasion by a migrating supraglacial rill. Negative correlations were evident at shorter lags (Table 2B).
271 The strongest negative correlations were invariably greater than the maximum positive correlation for the
272 same hole. For ΔV_w and I^* , the mean lag associated with maximum negative correlation was 3.59 ± 2.69
273 hr and between ΔV_w and T_a it was 5.28 ± 2.87 hr. Hole 1 was considered anomalous and omitted from
274 mean lag calculations.

275 For each hole ΔV_w was separated into daily increase (ΔV_w^+) and daily decrease (ΔV_w^-) identified as the
276 rising and falling limbs of the daily hydrographs. Discounting the late-season amplified fluctuations in
277 Hole 1, the maximum ΔV_w^+ in any hole during the measurement period was 40 cm^3 compared to an
278 average of 116 cm^3 of ΔV_w^+ required to fill the holes to capacity and cause the meniscus of the hole water
279 to reach the ice surface. Table 3 shows daily filling and emptying rates (i.e. rate of change of ΔV_w^+ and
280 ΔV_w^- respectively) for each hole averaged over the measurement period. The amplified filling and draining
281 of Hole 1 late in the measurement period caused the averages for that hole to be much higher than the
282 others, reflected in the high standard deviation. The correlation between fill and drainage rate varied
283 between the monitored holes across a full range from weak to strong: for Holes 1 and 8, fill and drainage
284 rates were strongly correlated while for Holes 2-6 Pearson-correlation coefficients varied between 0.01
285 and 0.63 (Table 3).

286 In all holes, the fill and drainage rates accelerated as the season progressed (except for Hole 5, in which
287 only ΔV_w^+ accelerated, and Hole 7 where rill invasion obscured late-season phenomena), although the
288 analysis in Table 4 illustrates that there was considerable variability, with the acceleration best described
289 by linear models with coefficients of determination (between 0.0014 and 0.6891) and p-values varying
290 widely between < 0.001 and 0.86. In Hole 1 only, an exponential model better explained the acceleration
291 in filling rates ($V_w = 0.1802e^{0.1363t}$, $r^2 = 0.82$). Interestingly, despite Hole 1 being anomalous in terms of its
292 amplified ΔV_w after the warm air phase, it shows the highest coefficient of determination for linear models
293 and by far the lowest p-values.

294 Superimposed upon ΔV_w for each hole were rapid, stochastic fluctuations and occasional high magnitude
295 outflow events henceforth referred to as sudden drainage events (SDEs: see solid triangles in Fig.2B).
296 These SDEs tended to occur in the morning, particularly between 6 and 9 am coinciding with sharp
297 increases in I^* and accelerated melt (Fig.2B). A total of 20 SDEs were observed, of which 14 closely
298 followed a sharp increase in I^* to $> 100 \text{ Wm}^{-2}$. The most prominent morning SDE accounted for 61% of
299 that day's total ΔV_w^- in just 6% of the total drainage time (this occurred late in the measurement period in
300 Hole 1). The remaining 6 SDEs occurred late in the afternoon, also closely following large increases in I^*
301 that resulted from shifting cloud cover.

302 Hydraulic conductivity in the weathering crust:

303 Following application of slug (Fig.3A) and bail (Fig.3B) tests, ΔV_w was measured in Holes 1-3 (slug tests)
304 and Holes 4-6 (bail tests). Slug and bail tests were undertaken between 9 and 11 am, therefore during
305 periods of falling V_w , during the first half of the measurement period. Additional slug tests and bail tests
306 were also carried out during the afternoon, however the rates of recharge were too great to accurately
307 measure (due to refilling outpacing bailing and drainage outpacing addition of water) and they are omitted
308 from analysis here. In bail tests using the 3 different extraction volumes, V_w invariably showed return
309 periods of less than 50-minutes. For slug tests in Holes 4 and 6, V_w showed return periods of less than
310 sixty minutes; however Hole 5 never regained its original V_w . In all holes the hydrological equilibration to
311 both slug and bail tests were invariably non-linear and explained well by logarithmic functions.

312 Slug and bail data were used to calculate K (Eq. 2) for each hole at five minute resolution (Table 5). In all
313 six holes K values responded to slug and bail tests in a non-linear fashion best described using a
314 logarithmic curve. Average K values (K_{av}) were broadly similar between all six holes and between slug
315 and bail tests (Table 5).

316 Melt Modelling:

317 Simulated surface melt rates for the study area, at 1 hr intervals, showed clear diurnal fluctuations in

318 antiphase with ΔV_w (Fig 2B). The average surface melt rate was 0.29 ± 0.63 mm w.e. h^{-1} , and no overall
319 trend was observed in this data. Radiative fluxes generally dominated the surface energy balance
320 (contributing on average 87.4% of total melt energy) although the relative contribution of radiative and
321 turbulent fluxes varied throughout the measurement period (Fig.2C and D). Later in the season, when
322 synoptic cloud conditions were more variable there were several periods of turbulent flux-dominated
323 energy balance, in particular during the Warm Air Phase (20th to 24th August), when cloud cover caused T_a
324 consistently above freezing whilst I^* was reduced. Comparison of the relative contribution of radiative
325 and turbulent fluxes to surface energy balance (Fig.2D) with ΔV_w (Fig.2B) shows that higher water levels
326 coincided with periods when turbulent fluxes had greater influence on the surface energy balance and
327 radiative-flux dominated energy balance coincided with lower water levels. The discussion below
328 therefore considers whether the ΔV_w antiphase with shortwave radiation flux indicated that subsurface
329 melting by shortwave radiation controlled cryoconite hole water levels.

330 **Discussion:**

331 Weathering crust hydrology:

332 Daily increases in I^* drive both surface and subsurface melt, creating gradients of increasing ice density
333 with depth and the development of the porous near-surface weathering crust ice (Muller and Keeler, 1969;
334 Fountain and Walder, 1998; Larson, 1978). Our modelling showed that the surface energy balance was
335 dominated by shortwave radiation fluxes during our observation period, showing that conditions widely
336 recognised to be conducive to subsurface melt and weathering crust development were prevalent. Water
337 level changes should therefore provide insights into the interaction between weathering crust development
338 and surface hydrology. Our monitoring in eight holes revealed synchronous diurnal fluctuations in ΔV_w
339 within the weathering crust that were, surprisingly, out of phase with both I^* and the melt rate. Therefore,
340 during the night, lower I^* enabled refreezing and contraction of interstitial pore spaces, greater flow-
341 impedance and greater V_w . Twelve of the fifteen hour lag between I^* and ΔV_w were therefore likely to be
342 explained by diurnal cycles of irradiance, whilst the remainder most likely represented the time taken for
343 I^* to remove the cold content of the near surface ice and cause internal melting in the weathering crust.
344 This was well-supported by stronger negative correlations at shorter lags (Table 3) which indicated
345 outflow induced by periods of subsurface melting during periods of greater shortwave radiation receipt. A
346 major perturbation to the conditions described above occurred during the warm air phase, when turbulent
347 heat fluxes dominated the surface energy balance and a general increase in ΔV_w in all cryoconite holes
348 was observed (Fig 2B). This change was entirely consistent with weathering crust decay which has
349 commonly been associated with turbulent-heat dominated energy balance, in contrast to periods of
350 weathering crust growth which are associated with periods of radiative-flux dominated energy balance
351 (Muller and Keeler, 1969; Schuster, 2001).

352 Coupling between cryoconite hole and weathering crust hydrology was characterised by non-linear
353 'overburdened' responses to slug and bail tests that suggested transmission through a saturated porous
354 medium. The re-equilibration rate declined as ΔV_w approached its pre-perturbation value, indicative of a
355 diminishing local hydraulic gradient. Furthermore, Hole 5 never regained pre-perturbation ΔV_w following
356 slug testing, which may have resulted from a rise in the weathering crust water table coinciding with the
357 slug test. Fluctuations in ΔV_w therefore likely reflected changes in the hydrologic regime of the glacier's
358 weathering crust. Our observations of ΔV_w therefore suggested daily cycles of storage and transmission
359 within the weathering crust, with enhanced storage at night and enhanced transmission during the day,
360 consistent with diurnal cycles of weathering crust growth and decay. Daily ΔV_w^+ generally outpaced ΔV_w^- ,
361 suggesting storage of water at hourly-daily timescales. Slug tests showed return times of 15-60 mins,
362 while bail tests re-equilibrated faster (15-40 mins), supporting short term hydrological storage in the
363 weathering crust.

364 K values were also broadly similar between all cryoconite holes, indicating relatively uniform weathering
365 crust permeability beyond the plot scale. In this study, data from slug and bail tests undertaken late in the
366 day were omitted due to return times being too rapid to accurately measure, which further indicated the
367 diurnal changes in weathering crust development through pore space change. The K values presented here

368 were comparable to results from other glaciers, although published values vary between 14.4 cm hr⁻¹ in
369 deeply weathered, fast-flowing glacier ice (Fountain and Walder, 1998) and 1.4×10^{-6} cm hr⁻¹ in slow-
370 moving ice, controlled by deformation at the scale of individual crystals (Lliboutry, 1971). Therefore,
371 local ice physics and crystallography appear to be important controls upon weathering crust hydrology.

372 A seasonal linear trend of decreasing V_w was common to all eight monitored holes (Table 1). This was not
373 thought to be a melt artefact since surface ablation and hole-floor melt were corrected for. The linearity of
374 the seasonal reduction in V_w suggested glacier-wide shifts in hydraulic gradient, because if local processes
375 dominated, hydraulic overburden would likely cause non-linear re-equilibration (as demonstrated by slug
376 and bail tests). Sobota (2009) also showed that, as might be expected, the zero degree isotherm was at its
377 deepest during late summer conditions on Waldemarbreen (Svalbard). Therefore, if propagation of the
378 zero-degree isotherm is driven by a dominance of I^* over sensible heat supply (as was the case in the
379 present study), then energy balance conditions can sustain a seasonal increase in weathering crust
380 thickness. The water storage potential and permeability of near-surface ice can therefore increase
381 accordingly, although Irvine-Fynn (2008) and Shea et al. (2005) note that this might be partially countered
382 by refreezing at depth during periods of reduced I^* . Progressive deepening of the weathering crust over
383 the observation period almost certainly explained the linear decrease in V_w in its cryoconite holes.

384 Sudden Drainage Events

385 Punctuating daily ΔV_w data were SDEs. These sudden discharge events accounted for an average of
386 39.6% (range 10 - 94%) of the net daily outflow in an average of 8.3% (range 0.5 - 54%) of the total
387 drainage time. A possible explanation was thermal cracking (Sanderson, 1978) or creep and fracture
388 (Schulson and Duval, 2009) of the hole floor. Thermal stresses can become appreciable in the top 3 m of
389 glacier ice and so cracking was linked to variations in the water tables of ice-lidded cryoconite holes upon
390 the East Antarctic Ice Sheet (Hodson et al. 2013). However, we suggest that the more modest temperature
391 fluctuations in Svalbard made cracking less likely and instead promote rapid adjustments in the
392 distribution of void spaces within the near-surface ice matrix. Since SDEs synchronised closely with
393 sudden, large increases in I^* , light-driven forcing of pore aperture adjustment seems plausible in
394 combination with any thermal cracking events that do occur. Several SDEs occurred simultaneously in
395 different holes (or in very close succession), but were not coincident with maximum ΔV_w in the holes.
396 Therefore forcing by energy balance conditions seemed more plausible than a hydro-fracturing process.

397 Our data therefore demonstrated how cryoconite holes act as natural piezometers and thus serve as
398 indicators of weathering crust hydrology and near-surface ice processes. Our measurements of ΔV_w in
399 cryoconite holes indicated diurnal and seasonal cycles of hydrological storage and drainage efficiency
400 coupled to weathering crust growth and decay. During colder periods when interstitial pores refreeze and
401 contract the weathering crust may provide longer term hydrological storage, especially when insulated
402 beneath ice lids or seasonal snow.

403 Residence of cryoconite in the weathering crust

404 Cryoconite holes also represent discrete units of supraglacial sediment storage within the weathering crust.
405 Movement of individual cryoconite granules through weathered ice was previously studied by Irvine-Fynn
406 et al. (2011) who found little evidence of significant cryoconite mass transfer resulting from weathering
407 crust hydrology on a Svalbard glacier surface, providing a context for the discussion of residence times for
408 granules in cryoconite holes.

409 Since cryoconite grain diameters are probably far in excess of interstitial pore apertures, transport of
410 cryoconite granules through hole walls was considered unlikely. The Hjulstrom-Sundborg curve
411 (Hjulstrom, 1935; Sundborg, 1956) was used to calculate a critical flow velocity of 114 cm hr⁻¹ required to
412 entrain the average granule measured in this study (mean diameter = 0.23 mm (n=15), density = 2.61 g
413 cm⁻³; source data not shown here). Given that K values showed a mean permeability of ice surrounding
414 cryoconite holes of 0.26 cm hr⁻¹ for normal flow, and a maximum of 0.65 cm hr⁻¹ during the most intense
415 SDE, threshold competence for entrainment of cryoconite was very unlikely, especially since our
416 estimated critical entrainment velocity does not account for packing density nor the cohesive properties of

417 biotic and biogenic material surrounding cryoconite grains. Therefore movement of granules within the
418 hole was unlikely to occur unless the melting rate of the floor became heterogeneous and created a slope.

419 Furthermore, no cryoconite holes in this study overfilled at any time during the measurement period,
420 despite changes in I^* and ablation. Throughout the season, for all holes except Hole 1 (which
421 demonstrated anomalous, amplified variations) ΔV_w was less than 40 cm^3 , compared to an average ΔV_w of
422 116 cm^3 required to fill cryoconite holes to capacity. This implied that even if grains were entrained into
423 suspension, redistribution onto the ice surface was very unlikely. Even at maximum ΔV_w in Hole 1, a
424 further 75.3 cm^3 of water was required to fill the hole. This illustrates that cryoconite holes represent
425 persistent stores of sediment within the weathering crust, making the importance of biological processes
426 within the granule (e.g. Cook et al. 2010) less surprising. Furthermore, in the event of overtopping and
427 redistribution of granules out of holes onto the ice surface, Irvine-Fynn et al. (2011) suggested that
428 continued transport down-glacier would also be slow.

429 Melt water inundation has been implicated in the literature as a mechanism of sediment evacuation from
430 cryoconite holes (e.g. Swan, 1992); however evidence here suggested overtopping of cryoconite holes,
431 and by extension removal of sediment by melt water, to be very infrequent (Takeuchi et al. 2010)
432 especially since these data represented mid-late summer melt. This supports previous assertions of multi-
433 year residence times for sediment in cryoconite holes (e.g. Hodson et al. 2007; Anesio et al. 2009; 2010;
434 Takeuchi et al. 2010). Exceptions may include invasion of cryoconite holes by supraglacial streams which
435 erased Holes 7 and 8 in this study.

436 Microbial mobility through the weathering crust

437 Irvine-Fynn and Edwards (2012) showed microbial cells, organic and inorganic nutrients are transported
438 through the weathering crust by melt water. Here, we have shown that hydrological processes have the
439 capacity to induce size-selectivity in the transport of particulate material and associated microorganisms.
440 We have also shown that the hydraulic conditions influence the rate of meltwater and therefore aqueous
441 nutrient propagation through the weathering crust. Transport of microbes through the weathering crust
442 probably therefore exposes them to varying light and nutrient conditions, influencing ecosystem structure
443 and function (Edwards et al. 2011; 2013a; 2014). Data presented here, therefore, suggests daily and
444 seasonal evolution of weathering crust permeability controls storage and transmission of microbes and
445 nutrients. Microbial community structure and function may be depth-dependent, with greater I^* near the
446 ice surface associated with photo-protective pigmentation and high rates of photosynthesis, and low I^* at
447 depth more likely associated with low-light adaptation and a tendency towards net heterotrophy (e.g.
448 Hodson et al. 2013). Studies of ciliates in cryoconite hole water found distinct stratification of species with
449 depth in the water column, suggesting that microscale heterogeneity in biotic and abiotic conditions with
450 depth influence microbial communities, and further indicating potential for hydrologic transmission of
451 living cells (Irvine-Fynn and Edwards, 2014). Since redistribution of microbes between micro-
452 environments is hydrologically controlled, weathering crust hydraulics likely influence supraglacial
453 microbial community structure and function. Consequently, spatiotemporal heterogeneity in hydraulic
454 transmission in the weathering crust should be explored in the context of nutrient and biomass delivery to
455 downstream ecosystems.

456 Being semi-persistent sediment stores, cryoconite holes are crucial habitats for life in the weathering crust.
457 Cryoconite holes could provide multiyear storage under favourable conditions for photosynthesis (Cook et
458 al. 2010), abundant nutrient supply from both autochthonous and allochthonous sources, and respite from
459 redistribution through the weathering crust, especially when cells become incorporated into cryoconite
460 aggregates. Cryoconite holes therefore represent sites of enhanced microbial activity, storage and nutrient
461 transformation within the weathering crust. Prolonged residence times are associated with stability and
462 extended periods of net carbon fixation on Arctic ice surfaces (Hodson et al. 2007; Anesio et al. 2009;
463 Cook et al. 2012) resulting in larger, more robust cryoconite aggregates (Langford et al. 2014). This
464 suggests cell fluxes into cryoconite holes may be important for determining surface albedo and
465 supraglacial carbon cycling.

466 Fluxes of cells out of cryoconite holes may also be important for supraglacial microbial dynamics. Export

467 of cells and dissolved nutrients is much more likely than cryoconite sediment due to the critical
468 competence for entrainment being far lower and the possibility for passage through interstitial pores.
469 Residence times for cells in cryoconite holes likely depends upon their incorporation into cryoconite
470 aggregates, degree of sheltering by layers of packed grains and the occurrence of SDEs. Enhanced flow
471 competence during SDEs might play an important role in mobilizing cells from storage in cryoconite
472 holes. Studies of fluvial ecology in other environments (e.g. Resh et al. 1988; Reice et al. 1990, Reice,
473 1994; Lake, 2000) suggest that disturbance, even below critical competence, can be a primary control
474 upon benthic ecosystem structure and function. This implies that the storage and release of cells from
475 cryoconite sediment is also tightly coupled with weathering crust hydraulic regime. This is supported by
476 growth rings in cryoconite cross-sections identified by Takeuchi et al. (2010) that suggest multi-year
477 (average 3.5 year) persistence of cryoconite organic matter prior to melt-water disturbance. Similarly,
478 Stibal et al. (2012) showed cryoconite granule size on the Greenland ice sheet to be coupled with surface
479 slope (a proxy for runoff velocity), implying periodic biomass removal by melt water disruption. In
480 general, cryoconite holes in flat, stable ice in the interior zones of large glaciers and ice sheets probably
481 provide more robust stores of biota than dynamic, rapidly melting ice in small glaciers and ice-sheet
482 margins. Langford et al. (2014) further found cryoconite aggregates in the interior of Longyearbreen
483 (Svalbard) to be smaller than at the sides due to enhanced hydraulic erosion by concentrated flow in a
484 central tract. Our data therefore adds to a growing literature supporting the importance of weathering crust
485 dynamics for supraglacial ecology, both as a medium for hydrologic transfer of cells and as a substrate for
486 cryoconite hole formation.

487 **Conclusions:**

488 Data from Austre Brøggerbreen described the mobility of water through the weathering crust and
489 confirmed that its behaviour is analogous to a shallow perched aquifer. Cryoconite holes were used as
490 natural piezometers to obtain time series of hydraulic changes within the aquifer, revealing a positive
491 correlation between radiative forcing of melt and drainage efficiency, and therefore a negative correlation
492 between radiation and hydrological storage and sometimes resulting in sudden drainage events (SDEs).
493 This was suggested to result from the contraction and dilation of interstitial pores due to radiative forcing
494 of night time refreezing and day time melting. A linear decrease in water levels in cryoconite holes was
495 also observed and attributed to the deepening of the weathering crust over the 3-week measurement
496 period. Cryoconite holes were shown to represent sites of prolonged cryoconite storage, which explains
497 why they are loci of enhanced microbial activity and biogeochemical cycling. Complex relationships
498 therefore likely exist between weathering crust growth and decay, environmental stresses, microbial
499 activity and hydraulic redistribution of nutrients and biomass. This study highlights the dynamic
500 weathering crust as a crucial component of the hydrology, microbial ecology and biogeochemistry of the
501 glacier ecosystem and glacierized regions.

502 **Acknowledgements:**

503 J. Cook acknowledges his UK National Environment Research Council (NERC) Doctoral Training
504 Grant (No. NE/G524152/1). A Edwards and M Sweet are thanked for helpful comments on draft
505 manuscripts.

507 **References:**

- 508 Amoozegar A, Warrick AW. 1986. Hydraulic conductivity in saturated soils: field methods. In Klute,
509 A (Ed) *Methods of Soil Analysis pt. 1*, American Society of Agronomy, WI. pp.735-798.
- 510 Anesio AM, Hodson AJ, Fritz A, Psenner R, Sattler B. 2007. High microbial activity on glaciers:
511 importance to the global carbon cycle, *Global Change Biology*, 15 (4): 955-960.
- 512 Anesio AM, Sattler B, Foreman C, Telling J, Hodson A, Tranter M, Psenner R. 2010. Carbon fluxes
513 through bacterial communities on glacier surfaces, *Annals of Glaciology*, 51 (56): 32-40.

- 514 Arnold NS, Rees WG. 2003. Self-similarity in glacier surface characteristics, *Journal of Glaciology*,
515 49, 547–554, doi:10.3189/172756503781830368.
- 516 Bagshaw EA, Tranter M, Fountain AG, Welch KA, Basagic H, Lyons WB. 2007. Biogeochemical
517 evolution of cryoconite holes on Canada Glacier, Taylor Valley, Antarctica, *Journal of Geophysical*
518 *Research*, 112, G04S35.
- 519 Barrand NE, James TD, Murray T. 2010. Spatiotemporal variability in elevation changes of two high-
520 Arctic valley glaciers. *Journal of Glaciology* 56 (199): 771–780.
- 521
- 522 Bear J. 1972. *Dynamics of Fluids in Porous Media*. Dover Publications. ISBN 0-486-65675-6.
- 523 Bouwer H, Rice RC. 1976. A slug test for determining hydraulic conductivity of unconfined aquifers
524 with completely or partially penetrating wells. *Water Resources Research*, 12 (3): 423-428.
- 525 Brandt RE, Warren SG. 1993. Solar-heating rates and temperature profiles in Antarctic snow and ice,
526 *Journal of Glaciology*, 39 (131): 99 – 110.
- 527 Brock BW, Arnold NS. 2000. A spreadsheet-based (Microsoft Excel) point surface energy balance
528 model for glacier and snow melt studies. *Earth Surface Processes and Landforms*, 25: 649–658.
- 529 Bruland O, Hagen JO. 2002. Glacial mass balance of Austre Brøggerbreen (Spitsbergen) 1971-1999,
530 modelled with a precipitation-runoff model. *Polar Research*, 21 (1): 109-121.
- 531 Cook J, Hodson A, Telling J, Anesio AM, Irvine-Fynn T, Bellas C. 2010. The mass–area relationship
532 within cryoconite holes and its implications for primary production. *Annals of Glaciology*, 51 (56):
533 106-110.
- 534 Cook JM, Hodson AJ, Anesio AM, Hanna E, Yallop M, Stiba, M, Telling J, Huybrechts P. 2012. An
535 improved estimate of microbially mediated carbon fluxes from the Greenland Ice Sheet. *Journal of*
536 *Glaciology*, 58(212), 1098–1108.
- 537 Cutler PM, Munro DS. 1996. Visible and near-infrared reflectivity during the ablation period on Peyto
538 Glacier, Alberta, Canada. *Journal of Glaciology*, 42 (141): 333-340.
- 539
- 540 Derikx L. 1971. The heat balance and associated runoff from an experimental site on the glacier
541 tongue, *International Association of Scientific Hydrology Publication*, 104, 59–69.
- 542 Edwards A, Anesio AM, Rassner SM, Sattler B, Hubbard B, Perkins WT, Young M, Griffith GW.
543 2011. Possible interactions between bacterial diversity, microbial activity and supraglacial hydrology
544 of cryoconite holes in Svalbard. *The ISME Journal*, 5: 150-160.
- 545 Edwards A, Pachebat JA, Swain M, Hegarty M, Hodson A, Irvine-Fynn TDL, Rassner SM, Sattler B.
546 2013a. A metagenomic snapshot of taxonomic and functional diversity in an alpine glacier cryoconite
547 ecosystem. *Environmental Research Letters*, 8 (035003): 11pp.
- 548 Edwards, A, Rassner SM, Anesio AM, Worgan HJ, Irvine-Fynn TD, Williams HW, Sattler B, Griffith
549 GW. 2013b. Contrasts between the cryoconite and ice-marginal bacterial communities of Svalbard
550 glaciers. *Polar Research*, 32, DOI: 10.3402/polar.v32i0.19468.
- 551 Edwards A, Mur L, Girdwood S, Anesio A, Stibal M, Rassner S, Hell K, Pachebat J, Post B, Bussell
552 J, Cameron S, Griffith G, Hodson A. 2014. Coupled cryoconite ecosystem structure-function

553 relationships are revealed by comparing bacterial communities in Alpine and Arctic glaciers. *FEMS*
554 *Microbial Ecology*, Doi: 10.1111/1574-6941.12283.

555 Fountain AG, Walder JS. 1998. Water flow through temperate glaciers. *Reviews of Geophysics*, 36
556 (3): 299-328.

557 Fountain AG, Tranter M, Nylén TH, Lewis KJ, Meuller DR. 2004. Evolution of cryoconite holes and
558 their contribution to meltwater runoff from glaciers in the McMurdo Dry Valleys, Antarctica. *Journal*
559 *of Glaciology*, 50 (168): 35-45.

560 Geiger R. 1965. *Das Klima der bodennahen Luftschicht*. Vierte Auflage. Braunschweig, Friedrich
561 Vieweg und Sohn. [English translation: *The climate near the ground*. Translated by Scripta Technica,
562 Inc. Cambridge, Mass., Harvard University Press, 1965.]

563 Hagen JO, Sætrang A. 1991. Radio-echo soundings of sub-polar glaciers with low frequency radar.
564 *Polar Research*, 9: 99-107.

565
566 Hanssen-Bauer I, Kristensen-Solis M, Steffensen EL. 1990. The climate of Spitsbergen. (Det Norske
567 Meteorologiske Institutt) DNMI Klima Rapp. 39.

568 Hjulström F. 1935. Studies of the morphological activity of rivers as illustrated by the river Fyris.
569 *Bulletin of Geology*, Institute of Uppsala, 25: 221-527.

570 Hodson AJ, Gurnell AM, Washington R, Tranter M, Clark MJ, Hagen JO. 1998. Meteorological and
571 runoff time-series characteristics in a small, high-Arctic glaciated basin, Svalbard. *Hydrological*
572 *Processes*, 12 (3): 509–526.

573
574 Hodson A, Tranter M, Gurnell A, Clark M, Hagen JO. 2002. The hydrochemistry of Bayelva, a high
575 Arctic proglacial stream in Svalbard *Journal of Hydrology*, 257: 91-114.

576
577 Hodson AJ, Anesio AM, Ng F, Watson R, Quirk J, Irvine-Fynn T, Dye A, Clark C, McCloy P, Kohler
578 J, Sattler B. 2007. A glacier respire: Quantifying the distribution and respiration CO₂ flux of
579 cryoconite across and entire Arctic supraglacial system. *Journal of Geophysical Research*, 112
580 (G04S36), doi: 10.1029/2007JG000452.

581 Hodson AJ, Anesio AM, Tranter M, Fountain AG, Osborn M, Priscu J, Laybourn-Parry J, Sattler B.
582 2008. *Glacial Ecosystems*, Ecological Monographs, 78 (1), 41-67.

583 Hodson A, Paterson H, Westwood K, Cameron K, Laybourn-Parry J. 2013. A blue-ice ecosystem on
584 the margins of the East Antarctic ice sheet. *Journal of Glaciology*, 59 (214): 255-268.

585 Hoffman MJ, Fountain AG, Liston GE. 2014. Near surface internal melting: a substantial mass loss on
586 Antarctic Dry Valley glaciers. *Journal of Glaciology*, 60 (220): 361-374.

587 Irvine-Fynn TDL, Moorman BJ, Williams JLM, Walter FSA. 2006. Seasonal changes in ground-
588 penetrating radar signature observed at a polythermal glacier, Bylot Island, Canada. *Earth Surface*
589 *Processes and Landforms*, 31: 892–909.

590 Irvine-Fynn TDI. 2008. Modelling runoff from the maritime arctic cryosphere: water storage and
591 routing at Midtré Lovénbreen. PhD thesis, University of Sheffield, 2008

592 Irvine-Fynn TDL, Hodson AJ, Moorman BJ, Vatne G, Hubbard AL. 2011. Polythermal Glacier
593 Hydrology: A review, *Reviews of Geophysics*, 49, RG4002.

594 Irvine-Fynn TDL, Edwards A, Newton S, Langford H, Rassner SM, Telling J, Anesio AM, Hodson
595 AJ. 2012. Microbial cell budgets of an Arctic glacier surface quantified using flow cytometry.
596 *Environmental Microbiology*, 14 (11): 2998-3012.

597 Irvine-Fynn TDL, Edwards AE. 2014. A frozen asset: The potential of flow cytometry in constraining
598 the glacial biome. *Cytometry Part A*, 85 (1): 3-7.

599 James TD, Murray T, Barrand NE, Sykes HJ, Fox AJ, King MA. 2012. Observations of enhanced
600 thinning in the upper reaches of Svalbard glaciers. *The Cryosphere*, 6 (6). 1369-1381.

601 Karlstrom L, Zok A, Manga M. 2014. Near-surface permeability in a supraglacial drainage basin on
602 the Llewellyn Glacier, Juneau Icefield, British Columbia. *The Cryosphere*, 8, 537-546.

603 LaChapelle E. 1959. Annual mass and energy exchange on the Blue glacier. *Journal of Geophysical*
604 *Research*. 64: 443-9.

605 LaChapelle E. 1961. Energy exchange measurements on the Blue Glacier. *International Association of*
606 *Scientific Hydrology*, 54: 302-310.

607 Lake PS. 2000. Disturbance, patchiness and diversity in streams. *Journal of the North American*
608 *Benthological Society*, 19 (4): 573-592.

609 Langford HJ, Irvine-Fynn TDL, Edwards A, Banwart SA, Hodson AJ. 2014. A spatial investigation of
610 the environmental controls over cryoconite aggregation on Longyearbreen glacier, Svalbard,
611 *Biogeosciences Discuss.*, 11, 3423-3463.

612 Larson GJ. 1977. Internal drainage of stagnant ice: Burroughs Glacier, Southeast Alaska, Institute of
613 Polar Studies Report 65. Ohio State University, Columbus, Ohio, pp. 33.

614 Larson GJ. 1978. Meltwater storage in a temperate glacier, Burroughs Glacier, Southeast Alaska.
615 Institute of Polar Studies Report 66. Ohio State University, Columbus, Ohio, pp. 56.
616

617 Liestøl O, Repp K, Wold B. 1980. Supra-glacial lakes in Spitsbergen, *Norsk Geografisk Tidsskrift*, 34,
618 89-92.

619 Liston GE, Winther JG, Bruland O, Elvehoy H, Sand K. 1999. Below-surface ice melt on the coastal
620 Antarctic ice sheet, *Journal of Glaciology*, 45 (150): 273-285.

621 Lliboutry LA. 1971. Permeability, brine content and temperature of temperate ice. *Journal of*
622 *Glaciology*, 10 (58): 15-29.

623 MacDonnell S, Fitzsimons S. 2008. The formation and hydrological significance of cryoconite holes.
624 *Progress in Physical Geography*, 32 (6): 595-610.

625 MacDonnell S, Fitzsimons S. 2012. Observations of cryoconite hole system processes on an Antarctic
626 glacier. *Revista Chilena de Historia Natural*, 85: 393-407

627 McIntyre NF. 1984. Cryoconite hole thermodynamics. *Canadian Journal of Earth Science*, 21 (2):
628 152-156.

- 629 Mieczan T, Gorniak D, Swiatecki A, Zdanowski M, Tarkowska-Kukuryk M, Adamczuk M. 2013.
630 Vertical microzonation of ciliates in cryoconite holes in Ecology Glacier, King George Island. Polish
631 polar Research, 34 (2): 201-212.
- 632 Mueller DR, Pollard WH. 2004. Gradient analysis of cryoconite ecosystems from two polar glaciers,
633 Polar Biology, 27, 66–74.
- 634 Muller F, Keeler CM. 1969. Errors in short-term ablation measurements on melting ice surfaces.
635 Journal of Glaciology, 8 (52): 91-105.
- 636 Munro DS. 1990. Comparison of melt energy computations and ablatometer measurements on
637 melting ice and snow. Arctic and Alpine Research, 22(2), 153–162.
- 638 Munro DS. 2011. Delays of supraglacial runoff from differently defined microbasin areas on the
639 Peyto Glacier. Hydrological Processes, 25 (19): 2983-2994.
- 640 Nowak A, Hodson A. 2014. Changes in meltwater chemistry over a 20-year period following a
641 thermal regime switch from polythermal to cold-based glaciation at Austre Brøggerbreen,
642 Svalbard. Polar Research, 33. DOI: 10.3402/polar.v33.22779
- 643 Nye JF. 1991. The rotting of temperate ice. Journal of crystal growth, 113 (3-4): 465-476.
- 644 Oke TR. 1987. Boundary layer climates. Second edition. London, Routledge Press. 1987.
- 645 Paultier BG, Dubnick A, Sharp M, Simpson AJ, Simpson MJ. 2013. Comparison of cryoconite
646 organic matter composition from Arctic and Antarctic glaciers at the molecular level. Geochimica et
647 Cosmochimica Acta, 104: 1-18.
- 648 Porter PR, Vatne G, Ng F, Irvine-Fynn TDL. 2010. Ice-marginal sediment delivery to the surface of a
649 high-arctic glacier: Austre Broggerbreen, Svalbard. Geografiska Annaler: Series A, Physical
650 Geography, 92A (4), pp. 437-449.
- 651 Reice SR, Wissmar RC, Naiman RJ. 1990. Disturbance regimes, resilience and recovery of animal
652 communities and habitats in lotic systems. Environmental Management, 14 (5): 647-659.
- 653 Reice SR. 1994. Nonequilibrium determinants of biological community structure. American Scientist,
654 82: 424-435.
- 655 Resh VH, Brown AV, Covich AP, Gurtz ME, Li HW, Minshall GW, Reice SR, Sheldon AL, Wallace
656 JB, Wissmar RC. 1988. The role of disturbance in stream ecology. Journal of the North American
657 Benthological Society, 74 (4): 433-455.
- 658 Rothlisberger H, Lang H. 1987. Glacial hydrology. In Gurnell, A.M. and M.J. Clark, eds. Glacio-
659 fluvial sediment transfer: an alpine perspective. Chichester, etc., Wiley, 207–284.
- 660 Sanderson TJO. 1978. Thermal stresses near the surface of a glacier. Journal of Glaciology, 20 (83):
661 257–283.
- 662 Schulson EM, Duval P. 2009. Creep and fracture of ice. Cambridge University Press, Cambridge, UK.
- 663 Schuster CJ. 2001. Weathering crust processes on melting glacier ice (Alberta, Canada). Theses and
664 Dissertations (Comprehensive), Wilfred Laurier University, Paper 489.

- 665 Shea JM, Anslow FS, Marshall SJ. 2005. Hydrometeorological relationships on Haig Glacier,
666 Alberta, Canada. *Annals of Glaciology*, 40: 52-60.
- 667 Shumskii PA. 1964. Principles of structural glaciology: the petrography of fresh-water ice as a
668 method of glaciological investigation. Dover Publications, 497pp.
- 669 Sobota I. 2009. The near-surface ice thermal structure of the Waldemarbreen, Svalbard. *Polish Polar*
670 *Research*, 30 (4): 317-338.
- 671 Stibal M, Telling J, Cook J, Man Mak K, Hodson A, Anesio A. 2012. Environmental controls upon
672 microbial abundance on the Greenland ice sheet: a multivariate analysis approach. *Microbial Ecology*,
673 63: 74-84.
- 674 Stuart G, Murray T, Gamble N, Hayes K, Hodson AJ. 2003. Characterization of englacial
675 channels by ground-penetrating radar: An example from Austre Broggerbreen, Svalbard. *Journal*
676 *of Geophysical Research-Solid Earth*, 108 (B11, 2525): 13 pp.
- 677 Sundborg A. 1956. The River Klarålvén: The morphological activity of flowing water erosion of the
678 stream bed. *Geografiska Annaler*, 38: 165-221.
- 679 Swan L. 1992. The aeolian biome. *Bioscience*, 42 (4): 262-270.
- 680 Takeuchi N, Kohshima Y, Seko K, Fujita K. 2000. Characteristics of cryoconite holes on a Himalayan
681 glacier, Yala Glacier central Nepal. *Bulletin of Glaciological Research*, 17: 51-59.
- 682 Takeuchi N, Nishiyama H, Li Z. 2010. Structure and formation process of cryoconite granules on
683 Ürümqi glacier No. 1, Tien Shan, China. *Annals of Glaciology*, 51 (56): 9-14.
- 684 Tetens O. 1930. Über einige meteorologische Begriffe, *Z. Geophys.* 6: 297–309.
- 685 Theakstone WH, Knudsen NT. Dye tracing tests of water movement at the glacier Austre
686 Okstindbreen, Norway. *Norsk Geografisk Tidsskrift*, 35: 21-28.
- 687
- 688 Tranter M, Fountain AG, Fritsen CH, Berry-Lyons W, Priscu JC, Statham PJ, Welch KA. 2004.
689 Extreme hydrochemical conditions in natural microcosms entombed within Antarctic ice.
690 *Hydrological Processes*, 18: 379–387.
- 691 Vatne G. 2001. Geometry of englacial water conduits, Austre Brøggerbreen, Svalbard. *Norsk*
692 *Geografisk Tidsskrift*, 55: 24-33.
- 693
- 694 Vatne G, Refsnes I. 2003. Channel pattern and geometry of englacial conduits. *Proceedings 6th*
695 *Internatinoal Symposium: Glacier caves and karst in Polar regions*. 181-188 pp.
- 696
- 697 Wakahama G, Kuroiwa D, Kobayashi D, Tanuma K, Endo Y, Mizuno Y, Kobayashi S. 1973.
698 Observations of permeating water through a glacier body, *Low Temperature Science*, 31A, 209–220.
- 699 Wharton RA, McKay CP, Simmons GM, Parker BC. 1985. Cryoconite holes on glaciers. *Bioscience*,
700 35: 449-503.
- 701 Wheler BA, Flowers GE. 2011. Glacier subsurface heat flux characterizations for energy balance
702 modelling in the Donjek Range, southwest Yukon, Canada. *Journal of Glaciology*, 57 (201): 121-133.

703 Wilhelm L, Singer GA, Fasching C, Battin TJ, Besemer K. 2013. Microbial biodiversity in glacier-fed
 704 streams. ISME Journal, 7: 1651 – 1660.

705 Zeng Q, Cao M, Feng X, Liang F, Chen X, Sheng W. 1984. A study of spectral reflection
 706 characteristics for snow, ice and water in the north of China, in: Hydrological Applications of Remote
 707 Sensing and Remote Data Transmission, edited by: Goodison, B. E., IAHS, 145, 451–462.

708 **Tables:**

709

Hole	Equation	r ² value
1	$V_w = -0.0004t + 0.4498$	0.21
2	$V_w = -0.0003t - 1.6185$	0.73
3	$V_w = -0.0005t - 1.4809$	0.78
4	$V_w = -0.0003t - 2.3209$	0.74
5	$V_w = -0.0004t - 0.7453$	0.79
6	$V_w = -0.0005t - 0.5904$	0.85
7	$V_w = -0.0009t - 0.4547$	0.93
8	$V_w = -0.0006t - 1.3092$	0.75

710

711 Table 1: linear regression coefficients for seasonal scale decrease in V.

712

A		T _a		IR	
Hole	Lag	R	Lag	R	
1	8.67	0.49	11	0.49	
2	18.67	0.42	17.25	0.37	
3	19.17	0.14	17.5	0.18	
4	13.67	0.39	12	0.48	
5	19.83	0.21	18.58	0.24	
6	16.25	0.22	14.75	0.34	
Mean	16.04	0.31	15.18	0.35	
σ	4.27	0.14	3.13	0.12	
B		T _a		IR	
Hole	Lag	R	Lag	R	
1	-3.08	-0.44	0.17	-0.56	
2	6.67	-0.33	5.25	-0.53	
3	8.50	-0.33	7.17	-0.25	
4	1.67	-0.42	1.00	-0.55	
5	6.67	-0.19	6.08	-0.27	
6	2.92	-0.45	1.92	-0.49	
Mean	5.28	-0.36	3.59	-0.44	
σ	2.87	-0.099	2.69	-0.14	

713

714 Table 2: A) Lag times (hours) at which the maximum positive correlation coefficient was observed, and
 715 the Pearson correlation coefficient (R) at that lag time, for each of Holes 1 – 6. Two-tailed t-tests
 716 invariably revealed significance at p<0.0001. B) Lag times (hours) at which the maximum negative

717 correlation coefficient was observed, and the Pearson correlation coefficient (R) at that lag time, for each
 718 of Holes 1-6. Two-tailed t-tests invariably revealed significance at $p < 0.0001$

719

Hole	Fill rate ($\text{mm}^3 \text{s}^{-1}$)	σ	Drainage rate ($\text{mm}^3 \text{s}^{-1}$)	σ	R
1	22.03	21.66	-29.34	24.76	0.88
2	7.50	5.57	-8.11	4.37	0.44
3	4.02	2.95	-5.48	4.79	0.19
4	5.14	4.62	-6.21	4.41	0.01
5	3.69	4.51	-3.99	1.62	0.19
6	2.14	1.98	-2.62	1.84	0.63
7	2.48	2.15	-2.48	0.64	0.56
8	1.06	3.25	-1.26	3.92	0.81

720

721 Table 3: Measurement-period average of daily fill rates and drainage rates for each hole and correlation
 722 coefficient between fill rate and drainage rate for each hole (uncertainty = 1σ ; R = Pearson correlation
 723 coefficient)

724

725

Hole	A		B	
	Equation	r^2	Equation	r^2
1	$0.00003t - 9.8044$	0.69	$-0.00004t + 6.5177$	0.67
2	$0.00004t + 3.5051$	0.21	$-0.00004t - 4.4608$	0.22
3	$0.0000003t - 3.69$	0.0039	$-0.000002t - 3.0366$	0.083
4	$0.000004t - 1.1225$	0.24	$-0.000001t - 4.6633$	0.039
5	$0.0000003t + 4.4844$	0.0013	$-0.0000004t - 3.6435$	0.014
6	$0.000002t + 0.4009$	0.244	$-0.000001t - 1.3274$	0.155
7	$0.000002t + 1.5792$	0.054	$-0.000001t - 3.0762$	0.268
8	$0.000003t - 0.295$	0.3284	$-0.000004t + 0.1086$	0.353

726

727 Table 4: Equations and linear regression coefficients for the changes in fill rate (A) and drainage rate (B)
 728 in each hole over the observation period.

729

730

Time (mins)	Hole number					
	1	2	3	4	5	6
5	-0.157	-1.479	3.78	-4.205	-2.38	-0.379
10	-0.0787	-0.843	2.48	-1.743	-0.924	-0.0283
15	-0.0754	-0.599	0.927	-1.063	-0.640	0.0198
20	0.0628	-0.477	0.498	-0.737	-0.488	0.0177
25	-0.0589	-0.394	0.259	-0.551	-0.366	0.0281
30	-0.0559		0.155	-0.440	-0.285	0.0235
35	-0.0517		0.0961	-0.369	-0.251	0.0233

40	-0.0463		0.0584	-0.320	-0.217	0.0439
45	-0.0382		0.0249	-0.280	-0.188	0.0484
50	-0.0353		0.0181	-0.248	-0.165	0.0483
55	-0.0320		0.00391	-0.222	-0.154	0.0460
60	-0.0294		0.00522	-0.198	-0.135	0.0432
65	-0.0279		0.00180		-0.127	0.0407
70	-0.0271		-0.00139		-0.118	0.0389
K_{av}	-0.0555 ± 0.034	-0.758 ± 0.437	0.554 ± 1.105	-0.865 ± 1.143	-0.294 ± 0.48	0.0055 ± 0.104

731

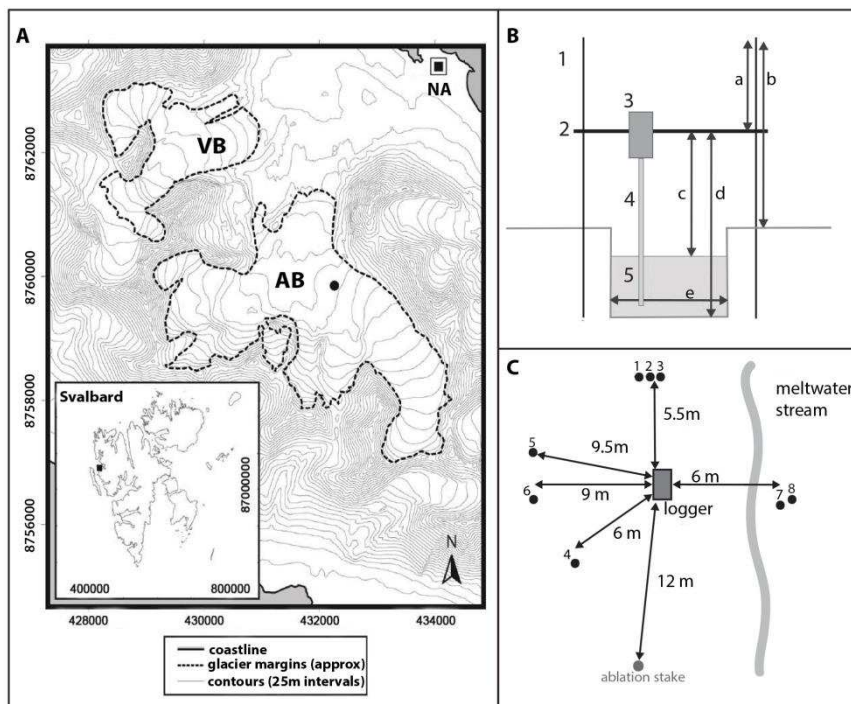
732

Table 5: K (cm hr^{-1}) at 5 minute resolution for slug and bail tests. Uncertainty = 1σ

733

734

735 **Figures:**



736

737

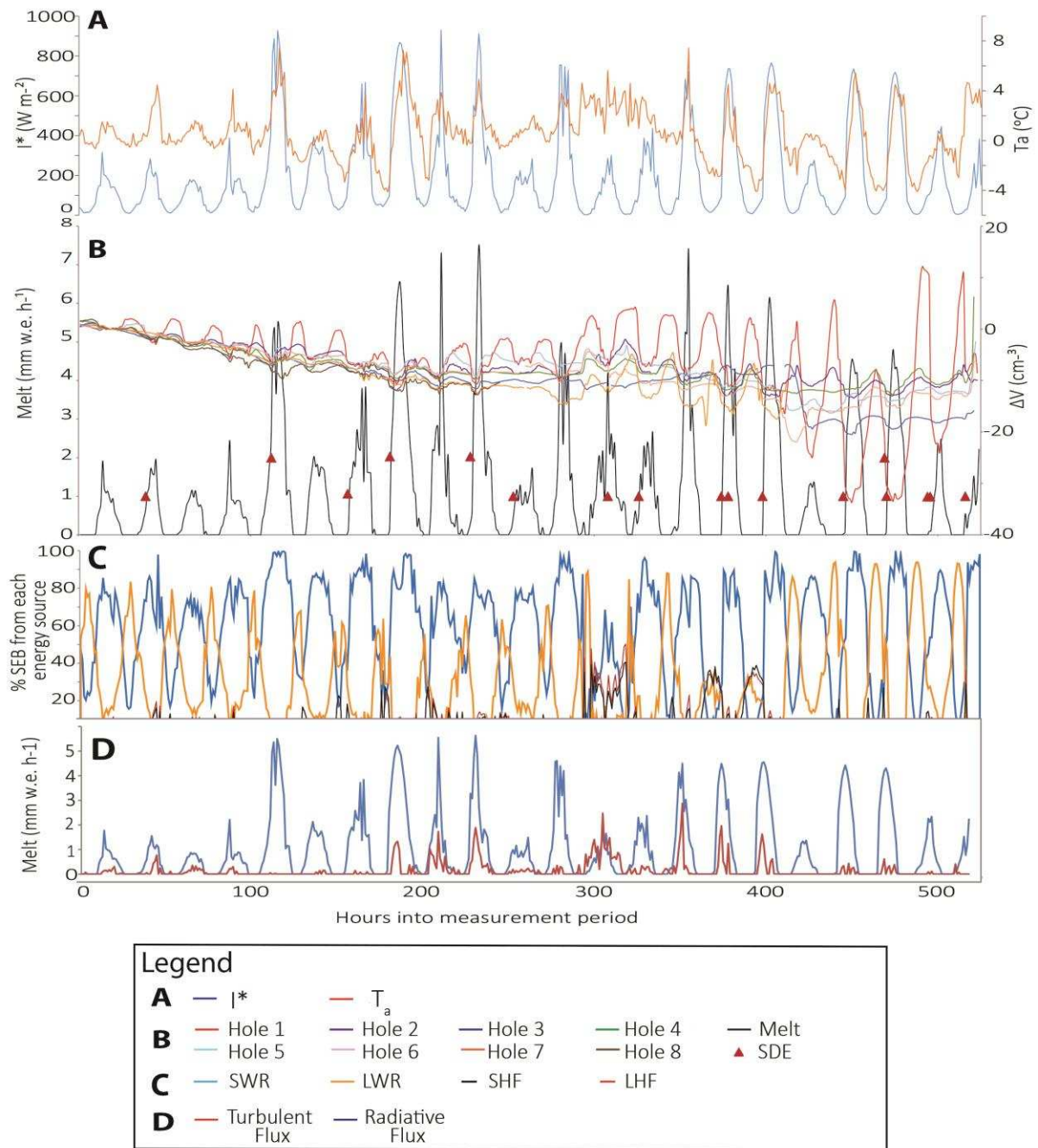
738

739

740

741

Figure 1. (A) map showing the location of Austre Brøggerbreen (AB) and the adjacent Vestre Brøggerbreen (VB), with the nearby town Ny Alesund (NA) also marked. The inset shows the position of these glaciers on the Svalbard archipelago. (B) Schematic of the goalpost structure and the associated measurements, where 1 = vertical rig pole, 2 = horizontal crossbar, 3 = water level sensor circuitry, 4 = water level sensor probe, 5 = cryoconite hole water, a = top of rig pole to crossbar, b = top of rig pole to ice surface, c = crossbar to hole water, d = crossbar to hole floor and e = hole width. (C) Map of field site

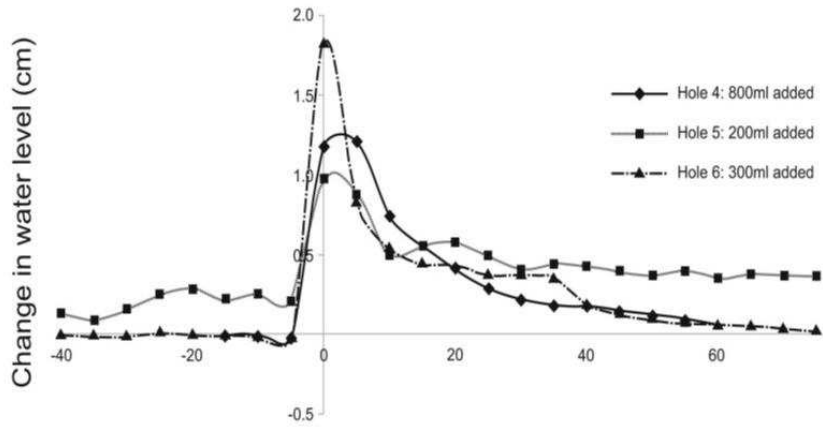


742

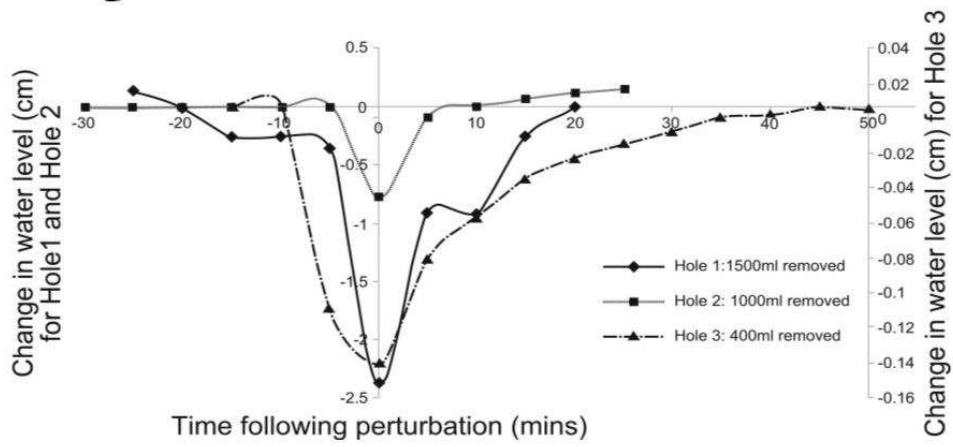
743 Figure 2. (A) I^* and T_a over the observation period and (B) melt rate, ΔV_w and SDEs for all holes over the observation period. Raised
 744 triangles indicate simultaneous sudden drainage events (SDEs) in two holes. (C) The percentage of the total surface energy balance (SEB)
 745 attributed to shortwave radiation (SWR), longwave radiation (LWR), sensible heat flux (SHF) and latent heat flux (LHF) throughout the
 746 observation period. Radiative fluxes are represented by filled areas, whereas turbulent fluxes are represented by lines for clarity. (D) Melt
 747 attributed to radiative fluxes and turbulent fluxes through the measurement period. The x-axis is shared by all four graphs.

748

A



B



749

750

Figure 3. (A) Return times for V_w in holes 4–6 following slug tests and (B) return times for V_w in holes 1–3 following bail tests